Infrared optical properties of the 10-K organic superconductor (BEDT-TTF)$_2$[Cu(NCS)$_2$] [where (BEDT-TTF) is bis(ethylenedithio)tetrathiafulvalene]

K. Kornelsen and J. E. Eldridge
Department of Physics, University of British Columbia, Vancouver, British Columbia, Canada V6T 1Z1

Hau H. Wang and Jack M. Williams
Chemistry and Materials Science Divisions, Argonne National Laboratory, Argonne, Illinois 60439
(Received 19 February 1991)

Low-temperature polarized bolometric absorption measurements have been performed on the $T_c = 10.4$ K organic superconductor κ-(BEDT-TTF)$_2$[Cu(NCS)$_2$], where BEDT-TTF is bis(ethylenedithio)tetrathiafulvalene. The ratio of the absorption at 5.3 K to that at 10.5 K from 10 to 40 cm^{-1} showed no evidence of a conventional BCS gap. Polarized-reflectivity measurements at temperatures between 10 and 295 K are also reported for both the protonated and deuterated compounds, between 200 and 8000 cm^{-1}. The 10-K spectra were calibrated by a technique of simultaneously measuring the reflectivity R and the absorptance, $1-R$. The resulting conductivities display vibrational features superimposed on an electronic background. This background shifts from mid-infrared interband transitions, when the dc conductivity is low, to far-infrared intraband transitions as the dc conductivity increases. The vibrations have been assigned to a mixture of normally inactive a_g modes and normally active b_{2u} modes of the BEDT-TTF molecule. A few of both types couple strongly to the charge carriers. One in particular has a very temperature-dependent frequency due to the changing intensity of the mid-infrared band.

I. INTRODUCTION

Several of the recently discovered organic superconductors have relatively high transition temperatures. The highest T_c of 11.6 K at ambient pressure is obtained in κ-(BEDT-TTF)$_2$Cu[N(CN)$_2$]Br, where BEDT-TTF is bis(ethylenedithio)tetrathiafulvalene, synthesized by Kini *et al.*[1] in 1990, while the previously highest T_c of 10.4 K (Refs. 2 and 3) belongs to κ-(BEDT-TTF)$_2$Cu(NCS)$_2$, where Cu(NCS)$_2$ is dithiocyanocuprate. This latter material is the subject of the present paper.

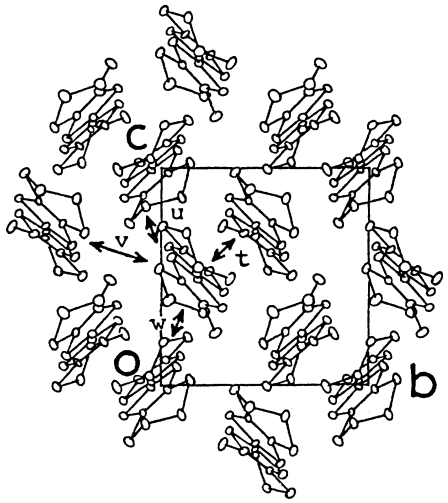

FIG. 1. The highly conducting *bc* plane of the κ-phase (ET)$_2$[Cu(NCS)$_2$] material, showing the pairs of ET molecules with alternating orientation. The long ET axis is perpendicular to the figure. The large circles are sulfur atoms, while the small are carbon.

These organic metals have electrical properties, which are two dimensional. The highly conducting planes are parallel to the larger sample surface and contain pairs of BEDT-TTF molecules (usually abbreviated to ET) arranged with alternating orientation to fill the plane (see Fig. 1). High electrical conductivity is allowed through the overlap between electronic orbitals of the sulphur atoms on neighboring ET molecules. In measurements of dc conductivity, the resistance perpendicular to the planes is lower by a factor of 600 compared to the nearly isotropic conductivity within the ET planes.[4,5] This two dimensionality is very similar to that observed in the ceramic high-T_c materials, leading to several recent comparisons.[6,7]

We have recently reported three communications of studies on (ET)$_2$Cu(NCS)$_2$. The first was a measurement of the optical properties of the protonated compound,[8] the second a study of the deuterated compound,[9] and the third a far-infrared search for the superconducting energy gap.[10] This paper consolidates those communications and elaborates on the findings.

II. FAR-INFRARED BOLOMETRIC ABSORPTION MEASUREMENTS

A. Introduction

BCS theory predicts a superconducting energy gap due to the Cooper-pair binding energy of $2\Delta = 3.5 k_B T_c$. Ear-

ly optical transmission measurements on superconducting lead and tin[11] demonstrated the existence of such a gap, while measurements on bulk lead samples[12–14] showed the almost perfect reflectivity in the spectral region below 2Δ. Structure above the gap due to phonons, and gaps greater than $3.5k_BT_c$ demonstrated the importance of strong coupling.

For the organic superconductors, a complete picture of the electron coupling mechanism has not yet emerged. Superconducting electron binding energies estimated from specific heat[15,16] and tunneling measurements[17,18] suggest the possibility of a strong coupling mechanism with $2\Delta/k_BT_c \approx 4$–4.5, but these results are strongly dependent on choices made in the interpretation of the data. An optical measurement of the superconducting gap could resolve the issue. Unfortunately, optical measurements near the superconducting gap energy are generally difficult with low-T_c materials in the form of small single crystals. They are usually good metals in the normal state with a reflectivity close to 100%. On going through T_c, one expects only a small increase in the reflectivity in the far-infrared region below 2Δ, where instrumental signals are always weak. Multiple sample reflections are often used to increase sensitivity, but for the small single-crystal organic superconductors this is not possible. Previous work on another organic superconductor, $(TMTSF)_2ClO_4$, by Ng *et al.*[19] used a mosaic of aligned single crystals in order to increase in the surface area for a reflectivity measurement. Good results were obtained, but diffraction effects introduced a considerable source of error. These diffraction effects reduce the collected signal when the wavelength of the far-infrared radiation becomes comparable to the crystal dimensions.

We have used the bolometric technique to measure the far-infrared absorption for the organic superconductor $(BEDT\text{-}TTF)_2[Cu(NCS)_2]$ at temperatures both at and below T_c. Bolometric measurements have been made using a small thermometer glued to the rear face of the organic crystal to measure the change in sample temperature due to absorption of far-infrared radiation, which is focused onto the sample at normal incidence. One advantage of the bolometric technique over conventional reflectivity measurements is that light from the spectrometer can easily be focused onto the sample without the need to collect the reflected light, which is spread by the diffraction effects mentioned. A more important benefit is that even though a highly reflecting sample will show only a small change in R going through T_c, our absorptance signal is directly proportional to $1-R$, since there is no transmisison, and it should therefore show a relatively large change. Absorption due to conventionally paired BCS conduction electrons should drop to almost zero for optical energies between 0 and $2\Delta = 3.53k_BT_c$ ($=25$ cm^{-1} in our case), when the temperature is well below T_c.

B. Experiment

The composite bolometer constructed for these experiments has been described in detail elsewhere.[10,20] A small doped silicon thermometer, sensitive at temperatures below about 11 K, is attached to the back of the $(ET)_2[Cu(NCS)_2]$ sample, which is then located at the focus of the beam of our Beckmann-RIIC far-infrared spectrometer. This type of thermometer has a resistance that decreases exponentially as the temperature increases from absolute zero. This characteristic, along with the increasing thermal conductivity of the gold support wires and heat capacity of the sample, reduces the sensitivity at higher temperatures and limits the maximum temperatures at which absorptance spectra can be measured.

In these measurements, one source of concern is the possibility that light might be absorbed by components of the detector other than the sample. There are three ways in which we were able to determine the significance of this leakage radiation. First, by measurement of the bolometer signal as a function of radiation chopping frequency, it was observed that direct thermometer heating had a very rapid response compared to that of the sample. Comparing the relative strengths of the high- and low-frequency bolometric response signals, it was possible to get a rough indication of the relative strength of the absorption due to leakage. Direct thermometer absorption also produces a spectrum with distinct characteristics, most easily distinguished by a large absorption peak at 360 cm^{-1}. This feature was observed in spectra recorded both before mounting the sample and in the leakage spectra measured at high chopping frequency. Finally, the signal measured due to leakage radiation is polarization independent, a distinguishing characteristic when compared with a polarization-dependent sample absorption. The result of these measurements showed that the signal obtained when the radiation was focused directly onto the front of the crystal, using a small rectangular aperture at the source, contained no more than 5% leakage, and when the signal was increased by using a larger aperture and allowing reflections from a light guide, the leakage was a maximum of 20% of the total.

C. Results

Measurements have been performed using several different samples with consistent results. The spectra shown here are from a single sample, with the absorption measured on the first and third coolings. On the first cooling, no cold filters were positioned before the sample in order to allow measurements over a wide spectral region. The spectrum shown in Fig. 2 was recorded with light polarized along the crystallographic b axis, 4-cm^{-1} resolution, and the light focused directly onto the sample surface at nearly normal incidence. In this case, the thermometer temperature was 5.5 K, but the presence of room-temperature background radiation brought the sample to a slightly higher temperature. Based on our measurement of the detector time constant, we estimate the actual sample temperature to be 7.5 K. The sample spectrum has been ratioed with a Golay background, giving the absorption axis an arbitrary scale but wavenumber-dependent accuracy to within $\pm 10\%$ above 30 cm^{-1}.

The spectrum in Fig. 2 shows that the absorption rises

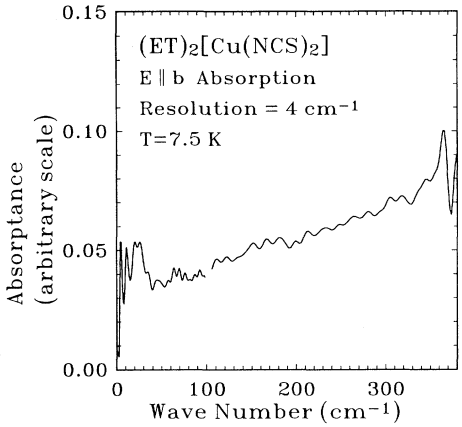

FIG. 2. The absorptance, $A=1-R$, obtained using a Golay detector to provide the reference spectrum. No cold filters have been used and the beam is focused on the sample. The upturn below 30 cm^{-1} is attributed to diffraction effects.

with increasing photon energy, but there are no obvious phonon features larger than the noise. The rise below 30 cm^{-1} is not reproducible and is attributed to a systematic difference in the diffraction affecting the Golay background and the sample spectra. A factor of 3 gain in signal could be obtained by increasing the size of the source aperture to allow light to reflect from the sides of a focusing light guide onto the sample. The noise in the best of these spectra was less than $\pm 3\%$ and, apart from the region below 30 cm^{-1}, which is affected by diffraction, a similarly featureless spectrum was obtained.

On the third cooling, a helium temperature fluorogold

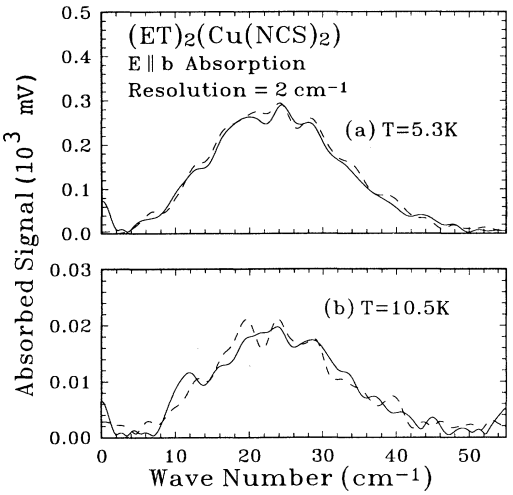

FIG. 3. The absorbed raw-power spectra using cold filters to remove all background radiation above 45 cm^{-1}. (They have not been ratioed with the Golay reference.) Two spectra at each temperature are superimposed to indicate the noise level.

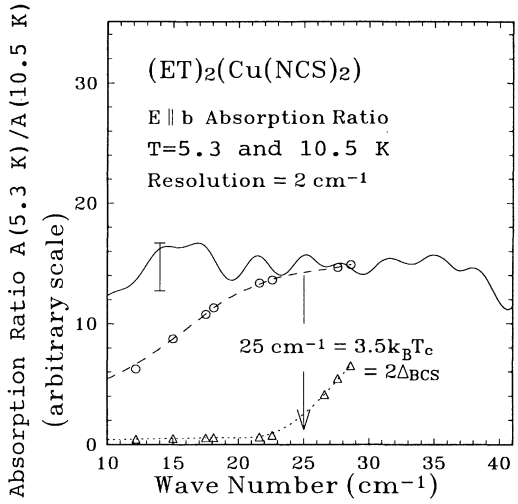

FIG. 4. The ratio of the 5.3- and 10.5-K spectra shown in Fig. 3. The BCS gap of 25 cm^{-1} is indicated. The triangles are aluminum data from Ref. 21, scaled to $T_c=10.5$ K. The circles are data scaled from the microwave results of Ref. 22 with the frequency dependence of aluminum.

optical filter in front of the sample removed all background radiation above 50 cm^{-1} and guaranteed a sample temperature well below the 10.4-K superconducting transition. Weak signal in this low-wave-number region and the addition of optical filters in the beam path made it necessary to use the focusing properties of the light guide to direct as much light as possible onto the sample surface. In the spectra shown in Figs. 3 and 4, radiation is again polarized with **E||b**, and spectral resolution is 2 cm^{-1}. The raw-power spectra obtained at temperatures of 10.5 and 5.3 K are shown in Fig. 3, with two spectra superimposed for each temperature to give an indication of the signal-to-noise level in the measurements. Each of the 10.5-K spectra shown in Fig. 3 is an average of two spectrometer scans, with each scan requiring a measuring time of 1 h. A ratio of the spectra measured below and at T_c in Fig. 4 shows no sign of any decrease in absorptance at the BCS gap energy of 25 cm^{-1}.

D. Discussion

Figure 4, while somewhat noisy, shows no drop in absorption at 5.3 K, which is $0.5T_c$, below the BCS gap of 25 cm^{-1}. For comparison, the triangles show the scaled data for aluminum[21] at $0.5T_c$. Of closer relevance are the circles, which are extrapolated from recent measurements of microwave surface impedance by Holczer *et al.*[22] At microwave and millimeter wave frequencies, the absorptance, A, is directly proportional to the surface resistance. The ratio of the surface resistance in the superconducting state to that in the normal state R_s/R_n was measured at 102 GHz (3 cm^{-1}) and found to be unusually high. At 5 K ($T/T_c=0.5$) the ratio was approximate-

ly 0.2. In the absence of data at other frequencies, one may tentatively use the frequency dependence of R_s/R_n for aluminum.[21] A ratio of 0.2 at an energy of $0.43k_BT_c$ (3 cm^{-1} in our case) corresponds for aluminum to the curve measured at a reduced temperature, T/T_c, not of 0.5 but of 0.9 instead. This curve has been scaled to correspond to a T_c of 10 K and is reproduced in our Fig. 4. While the effect is much smaller than one would anticipate for a reduced temperature of 0.5, it is two standard deviations away from our data and should be observable.

The simplest reasons why a gap might not be observed are that the sample is in the clean limit, or that the gap is an anisotropic function with nodes. For a clean limit superconductor, the conduction electrons in the normal state are scattered only occasionally, making the low-frequency Drude conductivity peak much narrower than 2Δ.[23] The best evidence for $(ET)_2[Cu(NCS)_2]$ being in the clean limit comes from measurements of the Shubnikov–de Haas effect.[24] This technique provides a fairly direct measurement of the conduction-electron scattering time and gives a clean limit result of $\tau=(3\pm1)\times10^{-12}$ s or $1/\tau\approx0.3k_BT_c=2$ cm^{-1}.

There are conflicting reports regarding the possibility of $(ET)_2[Cu(NCS)_2]$ having an anisotropic energy gap with nodes. If there is a node in the gap function, it is possible for photons of arbitrarily low energy to excite an electronic transition across the superconducting gap. Evidence for nodes in the gap function comes from the power-law dependence of the magnetic penetration depth $\lambda(T)$ as derived from susceptibility measurements.[25] This result is not confirmed in measurements of $\lambda(T)$ using the muon-spin-relaxation (μ^+SR) technique, which show no such power-law behavior.[26]

III. MID-INFRARED REFLECTIVITY MEASUREMENTS

A. Introduction

Several studies of the optical properties of $(ET)_2Cu(NCS)_2$ have been reported. Most of them were performed at room-temperature only.[27–31] Several of them include deuterated data[27,30,31] The only other low-temperature study of which we are aware is a low-resolution one by Ugawa *et al.*,[32,33] which went down in temperature to 25 K and in energy to 500 cm^{-1}, and from which no conductivity was extracted.

We have measured the power reflectivity R from 200 to 6000 cm^{-1} with a resolution of 2 cm^{-1}, for polarizations **E**||**b** and **E**||**c**, and at temperatures between 12 and 295 K. We then used the bolometric data of Sec. II to extend R down to 30 cm^{-1} at 12 K. We have recently calibrated R with an accuracy greater than that normally possible by using a technique of simultaneously measuring both the reflectivity and the absorptance. We present this technique here.

In our earlier report[8] we analyzed the conductivity in terms of a Drude model. We now present an interpretation based on interband transitions, using published electronic energy bands.

We repeated the measurements with deuterated crystals in order to assign the sharp vibrational features. These appear to be a mixture of totally symmetric (a_g) modes of ET, activated by electronic coupling, and normally active b_{2u} modes, one of which appears to be also coupling to the electrons. It is interesting to watch the frequency of the strongest a_g mode shift in response to changes in the electronic background.

B. Experiment

Data were taken with a Bruker IFS 113V Fourier spectrometer, using a 4-K doped-germanium bolometer with a Mylar beam splitter in the far infrared, and a mercury cadmium telluride detector with a KBr beam splitter in the mid infrared. The refrigerator was an Air-Products Heli-tran with a cold finger and a room-temperature CsI vacuum shroud window. The custom-designed reflectivity module has been described elsewhere.[34] R values were initially calibrated by comparison with those obtained from a freshly exposed aluminum-on-glass mirror and using the published R values for aluminum.[35] The samples were single crystals supported by gold wires and with a small doped-silicon thermometer attached to the rear face, as described in Sec. II. This told us the temperature of the crystal to within 0.1 K and allowed us to switch between reflectivity measurements and bolometric measurements.

The absolute accuracy of the measured reflectivity is very important for reliable derivation of the optical conductivity using a Kramers-Kronig analysis. By comparing the far-infrared and mid-infrared spectra in the regions of overlap, and by comparing spectra taken from different samples, we have found errors as high as 6%.

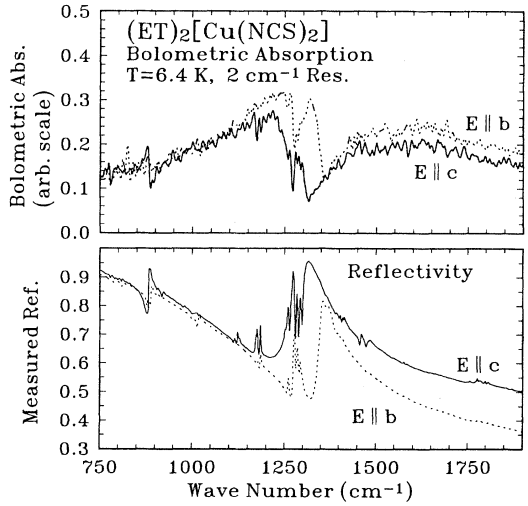

FIG. 5. The upper figure shows the polarized absorptance, $A=1-R$, in the mid-infrared, measured by the bolometric technique. It is seen to correspond well with the polarized reflectivity, shown in the lower figure, which was measured from the same sample in consecutive scans in the same experiment. These data were used to calibrate the reflectivity to within 1.5%.

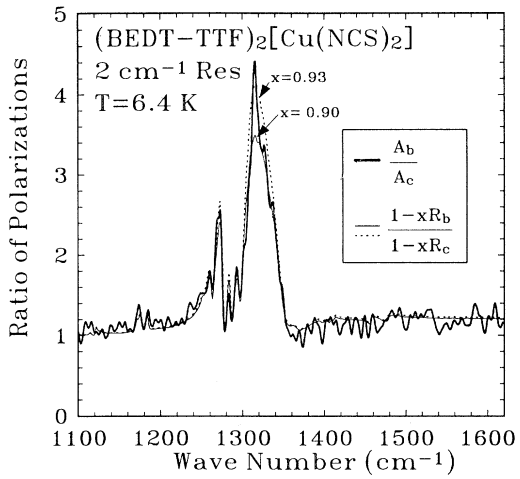

FIG. 6. The ratio of the two polarizations shown in Fig. 5. The bold line is the ratio of the absorptances A. The dashed and light lines are the ratios of $(1-xR)$, where x is a correction factor of 0.9 and 0.93, respectively.

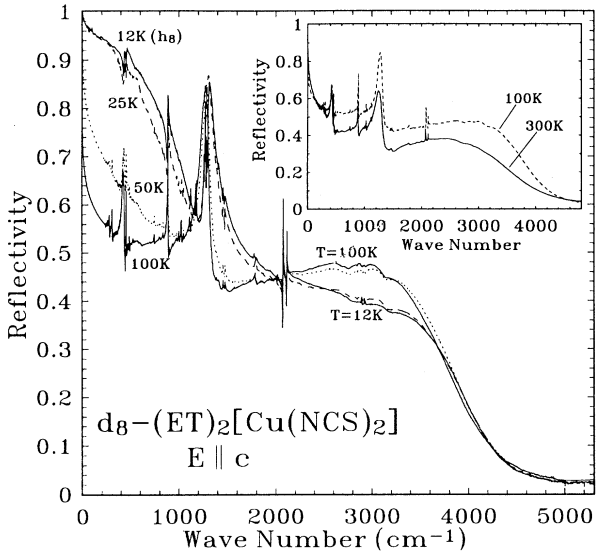

FIG. 7. The E||c power reflectivity for the deuterated compound at 295, 100, 50, and 25 K, and for the protonated compound at 12 K.

(It is known that the reflectivity decreases upon thermal cycling,[20] and so all the data shown here has been recorded on the first cooling cycle.) In order to reduce this uncertainty we obtained mid-infrared reflectivity and bolometric absorption spectra from the same sample, as shown in Fig. 5. The absorption spectra have an arbitrary scale but have been ratioed with the aluminum background in order to correct for the incident-beam polarization. The absolute absorptance A is equal to $1-R$, since there is no transmission, and Fig. 5 shows this correspondence convincingly. There is a finite time constant for the bolometric response, however, which causes the absorption spectra to fall above 1500 cm^{-1} instead of rising. (This is because these measurements were performed in the rapid-scan Bruker interferometer, as opposed to the Beckman used in Sec. II, which has a fixed chopping frequency.) Nevertheless, around 1300 cm^{-1}, the polarization dependence allows us to solve the following equation for x, the correction factor,

$$\frac{A_b}{A_c}=\frac{1-R_b}{1-R_c}=\frac{1-xR_{b,\mathrm{meas}}}{1-xR_{c,\mathrm{meas}}} . \quad (1)$$

Figure 6 shows that a good fit is obtained between the two ratios with $x=0.93\pm0.015$. This accuracy of 1.5% has the greatest impact in the far-infrared, where $1-R$ is small.

C. Results

Figures 7 and 8 show the power reflectivities for E||c and E||b, respectively, for temperatures of 295, 100, 50, 25, and 12 K. The resulting conductivities after Kramers-Kronig analyses are shown in Figs. 9, 10, and 11. The far-infrared conductivities agree reasonably well with the measured dc conductivities[32,4] of 20–40 $(\Omega\,\mathrm{cm})^{-1}$ at 295 K, 3–50 $(\Omega\ \mathrm{cm}\ )^{-1}$ at 100 K, 25–300 $(\Omega\,\mathrm{cm})^{-1}$ at 50 K and 1000–2500 $(\Omega\,\mathrm{cm})^{-1}$ at 25 K. Our 25- and 12-K conductivity spectra have zero-frequency intercepts at approximately 4500 $(\Omega\ \mathrm{cm}\ )^{-1}$, with the low-frequency peak having a half width of 40 cm^{-1}. A factor of 2 uncertainty in our extrapolated dc values and half widths results from the 1.5% accuracy in R. Figures 9 and 10 show that when the dc conductivity

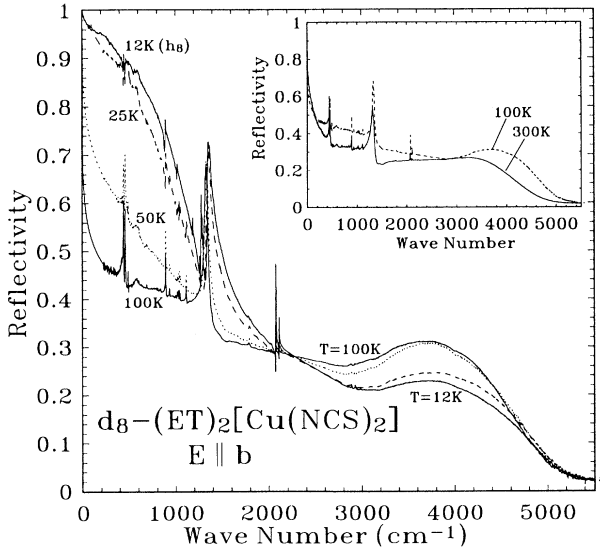

FIG. 8. The E||b power reflectivity for the deuterated compound 295, 100, 50, and 25 K, and for the protonated compound at 12 K.

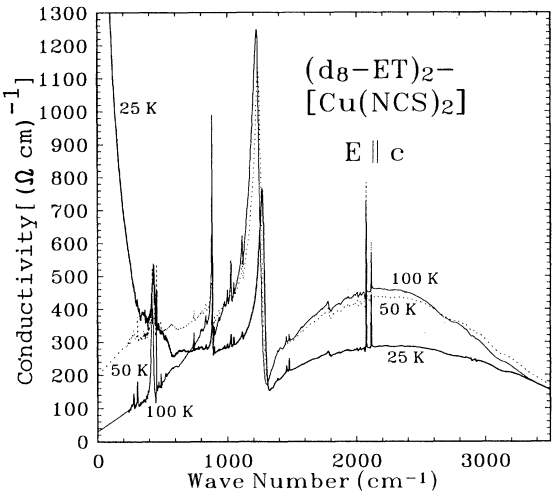

FIG. 9. The conductivity of the deuterated compound at 100, 50, and 25 K for **E**||**c**.

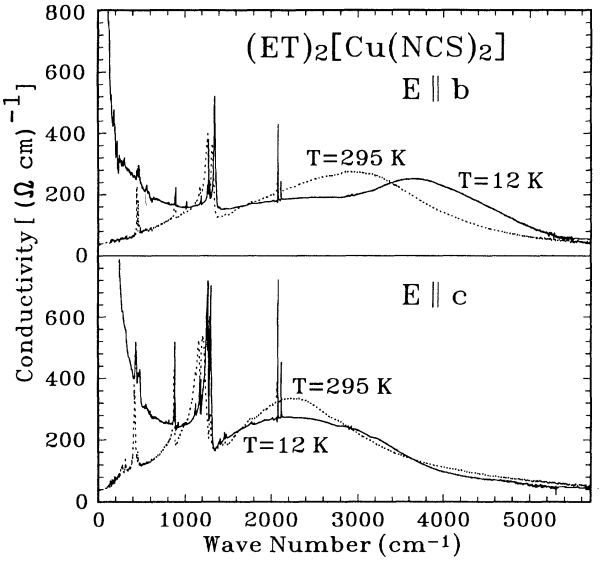

FIG. 11. The conductivity of the protonated compound at room temperature and at low temperature.

is a minimum, at 100 K, the mid-infrared peak is a maximum. (100 K is the temperature of the phase transition observed in thermopower measurements by Gartner *et al.*[36]) As the temperature drops below 100 K the far-infrared conductivity rises, while the mid-infrared conductivity drops, following a sum-rule relationship.

D. Electronic spectrum

We interpret the broad spectrum to be a combination of a far-infrared contribution from intraband transitions and a mid-infrared interband contribution. Figure 12 shows the band structure of κ-$(ET)_2Cu(NCS)_2$ calculated by Jung *et al.*[37] and Saito.[25] The general reliability of the band calculations is confirmed by successful predictions for the characteristics observed in Shubnikov–de Haas and thermopower experiments.[38–40] Interband transitions will take place vertically from the filled bands below the Fermi level to the empty ones above. The density of states increases as one moves away from the origin Γ towards the zone boundaries at Z and Y. The polariza-

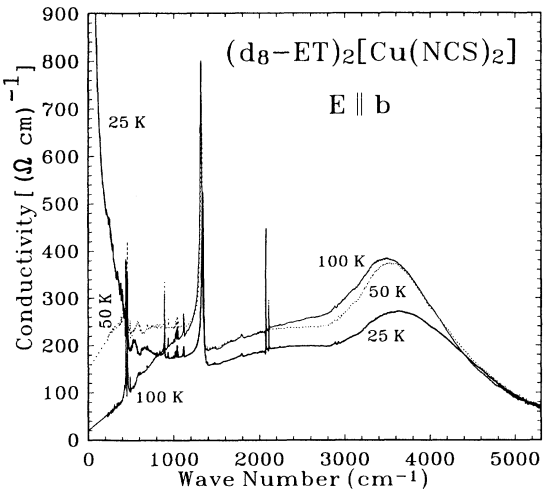

FIG. 10. The conductivity of the deuterated compound at 100, 50, and 25 K for **E**||**b**.

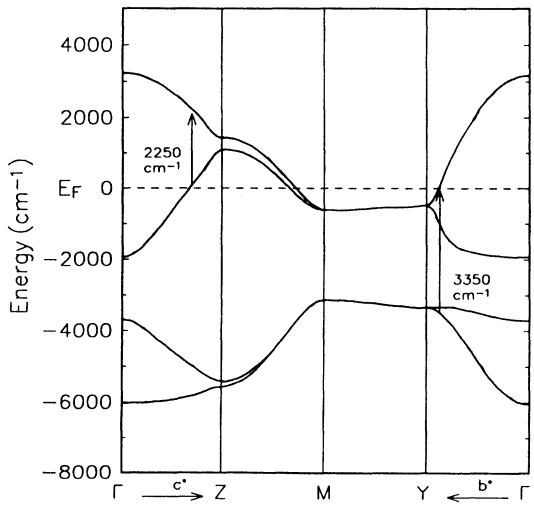

FIG. 12. The electronic band structure of $(ET)_2[Cu(NCS)_2]$ at 100 K from Ref. 37. The c^* direction is from Γ to Z and the b^* direction from Γ to Y. Arrows indicate transitions in regions where the density of states is expected to be high, giving broad peaks in the conductivity spectra with the frequencies indicated.

tion dependence arises from the scalar product between the electron wave vector and the electric field **E**. One therefore expects the **E**||**c** spectrum to be determined by the branches from Γ to Z, with the greatest contribution coming from the region closest to Z. For the upper bands this is at the intersection with the Fermi level giving a peak at 2250 cm^{-1}, as indicated by the arrow. The mid-infrared peak for **E**||**c** in Fig. 9 is indeed seem to be approximately 2200 cm^{-1}. Similarly, the **E**||**b** mid-ir spectrum will be dominated by the branches from Γ to Y with the peaks occurring from transitions near Y. The closest point is the intersection with the Fermi level. The upper two bands will contribute beginning at approximately 1000 cm^{-1}, while transitions from the lower two bands to the uppermost band should peak at 3350 cm^{-1}. Figure 10 shows that for **E**||**b** the peak occurs around 3500 cm^{-1}. No feature is seen at 1000 cm^{-1}, but a hump is obvious at 2000 cm^{-1}. This is probably due to transitions between the upper two bands slightly away from where the arrow is drawn and where the joint density of states may be greater. Detailed calculations are currently in progress.[41]

E. Vibrational assignments

Figures 13 and 14 show expanded portions of the conductivity spectra in which the vibrational features are predominantly found. The upper curves are the 25-K deuterated spectra, while the lower ones are the 12-K protonated spectra. Figures 15 and 16 show even more expanded portions of the protonated spectra in the vicinity of the largest vibrational feature, as a function of temperature. The dashed curves at 295 and 30 K are the superimposed deuterated spectra showing this feature in the absence of an interfering C—H mode of ET.

Before discussing the assignments, we show in Fig. 17(a) the molecular axes notation and the associated symmetry species. Figure 17(c) shows the pairs of ET mole-

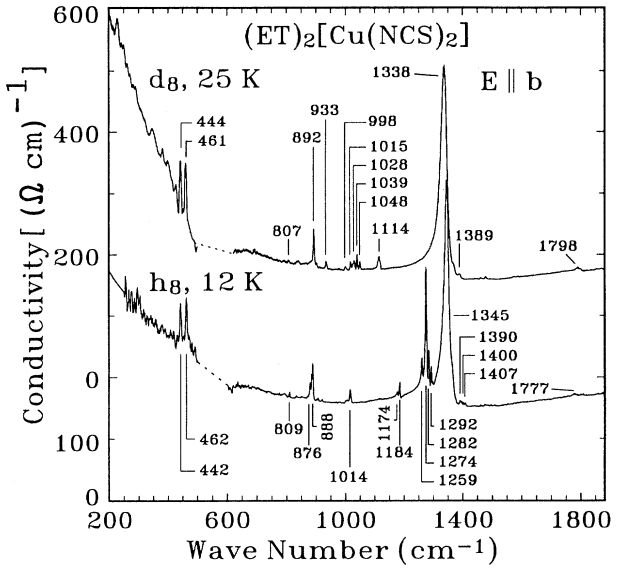

FIG. 14. Expanded portions of the **E**||**b** conductivity spectra of the deuterated compound at 25 K (upper curve) and the protonated compound at 12 K (lower curve), displaced for clarity. The indicated phonon features are listed in Table I.

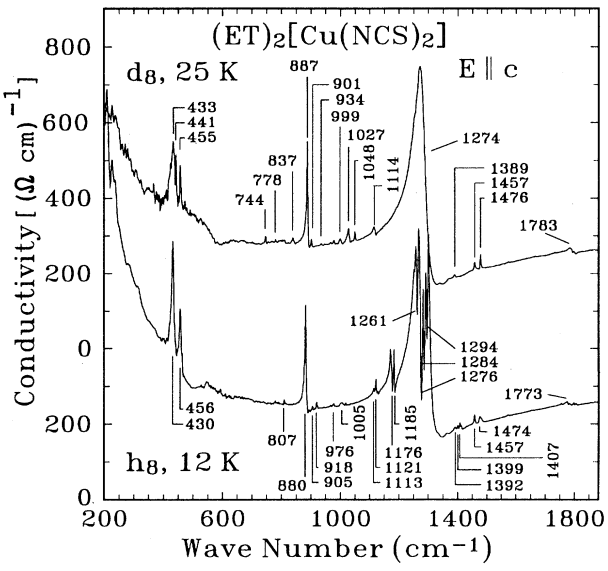

FIG. 13. Expanded portions of the **E**||**c** conductivity spectra of the deuterated compound at 25 K (upper curve) and the protonated compound at 12 K (lower curve), displaced for clarity. The indicated phonon features are listed in Table I.

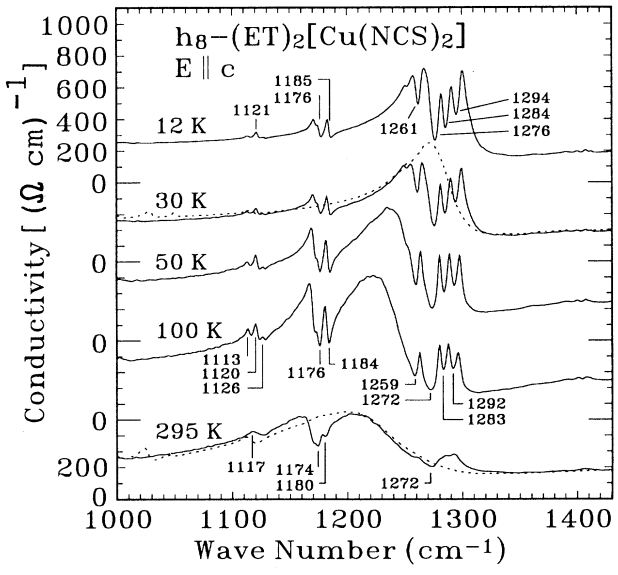

FIG. 15. Expanded portions of the **E**||**c** conductivity in the region of the strong ν_3 (a_g) resonance, as a function of temperature. The dashed curves at 295 and 30 K are from the deuterated compound showing the resonance in the absence of the interfering C–H vibrations.

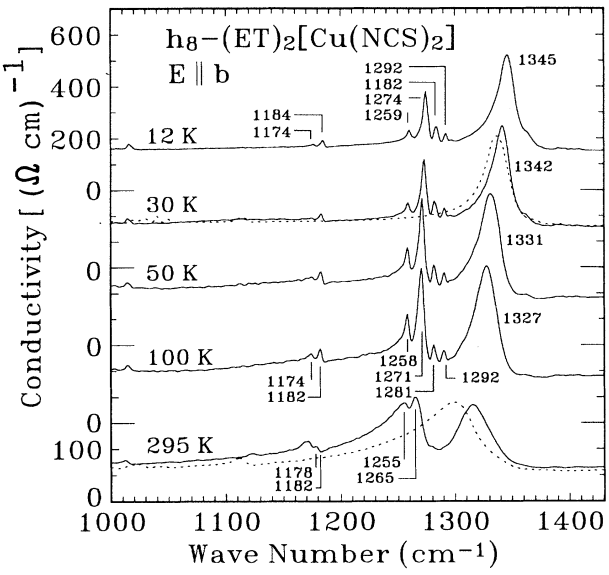

FIG. 16. Expanded portions of the **E||b** conductivity in the region of the strong ν_3 (a_g) resonance, as a function of temperature. The dashed curves at 295 and 30 K are from the deuterated compound showing the resonance in the absence of the interfering C–H vibrations.

cules arranged in the *bc* plane, which is the plane of our crystal face. The ET molecules are viewed end on, i.e., their long axis is almost perpendicular to the *bc* plane. Thus one would expect to see b_{2u} and b_{3u} normally active modes but not b_{1u}. A b_{2u} mode is drawn in Fig. 17(b), while the b_{3u} modes are out of plane. Because the

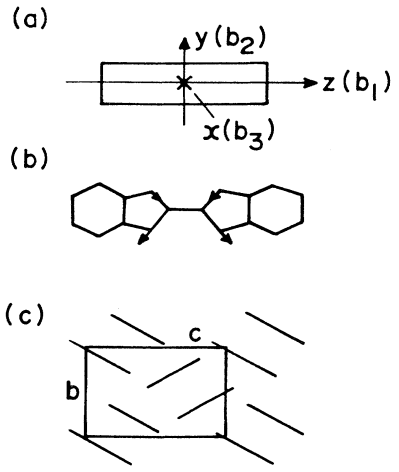

FIG. 17. (a) The molecular axes notation and the associated symmetry species; (b) an approximate representation of the ν_{49} (b_{2u}) normal mode, and (c) a sketch of the unit cell in the *bc* plane showing the end views of the molecular dimers.

ET molecules have a preferred orientation parallel to the *c* axis, the proportionality factor for coupling to the incident radiation is greater for b_{2u} modes in the **E||c** polarization than it is for **E||b**.

Table I lists all the features indicated in Figs. 13–16 plus a few at higher energies. The frequency and strength are indicated for both polarizations, along with the experimental isotope shift Δ, assuming a correct correlation between the features in the two spectra. The final column lists our assignment along with the calculated frequency for the ET cation from Kozlov, Pokhodnia, and Yurchenko[42] and the calculated isotope shift of the neutral molecule from the same authors.[43]

The largest feature is at 1274 cm^{-1} in the top curve of Fig. 13. The position of the peak in the protonated spectra is obscured by the Fermi resonances with another vibration, but the isotope shift is clearly small. It is generally agreed that it is due to a totally symmetric ET vibration involving the central C=C bond, either ν_2 or ν_3. Since the calculated electron molecular vibration coupling constant (EMVC) for ν_3 (a_g) is by far the greatest of any a_g mode,[42] we have assigned this large feature near 1300 cm^{-1} to ν_3 (a_g). Due to this coupling there is a large frequency shift down from the calculated frequency of 1427 cm^{-1}. This shift is less for **E||b**) ($\sim$127 cm^{-1} at 295 K) than for **E||c** ($\sim$227 cm^{-1} at 295 K) because the mid-infrared electronic band is further away. Figures 15 and 16 both show that this shift decreases as the temperature is lowered below 100 K and the mid-infrared band loses strength.

The next largest feature in the **E||c** spectrum of Fig. 13 is at 880 cm^{-1} (h_8-ET) and has a positive isotope shift to 887 cm^{-1} (d_8-ET). All other optical studies, which have considered the vibrations, have assigned this to the totally symmetric C–S stretching ET vibration ν_7 (a_g). According to the calculations, however, this mode would have an isotope shift of -108 cm^{-1}.[43] Indeed, in the h_8-ET Raman spectrum, a very weak feature at 911 cm^{-1}, is assigned to ν_7 (a_g) with the corresponding feature occurring at 794 cm^{-1} in the deuterated spectrum.[43] These are close to the wave numbers of the very weak features we have assigned to ν_7 (a_g) in Table I. No feature close to 911 cm^{-1} is reported in the deuterated Raman spectrum. The only mode with a calculated frequency close to 880 cm^{-1} and a zero isotope shift is ν_{49} (b_{2u}),[43] the asymmetric C–S stretching vibration illustrated in Fig. 17(b). The large intensity observed in Fig. 13 for **E||c** indicates a coupling to the electrons, and the nature of the mode points to the electrons oscillating between the differently oriented dimers, rather than between molecules in a dimer, or between similarly oriented dimers. Other examples of EMV coupling with normally active modes were found in TTF-TCNQ (where TCNQ is tetracyanoquinodimethane) (Ref. 45) and of electron coupling with a lattice vibration in $(TMTSF)_2ReO_4$ (where TMTSF is tetramethyltetraselenafulvalene).[46] These two, however, were charge-density-wave insulators, rather than a synthetic metal, which is the case here. Another indication of electron-coupling to the b_{2u} mode is the clear presence of the first overtone near 1780 cm^{-1} in all

TABLE I. Frequencies and assignments of the vibrational features for protonated and deuterated $(ET)_2[Cu(NCS)_2]$. Sample temperatures were 12 and 25 K for the protonated (h_{8-}) and deuterated (d_{8-}) samples, respectively. All frequencies are in cm^{-1}. vs is very strong, s is strong, m is medium, w is weak, vw is very weak, vvw is very very weak, and * is antiresonance dip. Where features are doublets or quartets, the assignment is listed beside the highest frequency only. Δ is the experimental isotopic frequency shift.

E‖b			E‖c					
h_{8-}	d_{8-}	Δ	h_{8-}	d_{8-}	Δ	Assignment	Calc. freq.[a]	Calc. shift[b]
2930vw	2175vvw	−755	2930vw	2175vvw	−755	$\nu_1(a_g)$	2912	−722
2891vw	2150vvw	−741	2891vw					
2921vw	2924vw	+3				$2\nu_3(a_g)$	2854	0
2885vw	2885vw	0						
2107s	2107s		2113s	2113s		ν (CN)		
2074s	2074s		2074s	2074s		ν (CN)	2074[c]	
1777vw	1789vw	+12	1773vw	1783vw	+10	$2\nu_{49}$ (b_{2u})	1796	−2
			1474w	1476w	+2	ν_2 (a_g)	1465	0
			1457w	1457w	0			
1407vw	1114w	−293	1407w	1114w	−293	ν_4 (a_g)	1421	−274
1400vw			1399w					
1390vw	1389vw		1392vw	1389vw	−3			
1345s	1338s	−7	≈1276vs	1274vs	≈−2	ν_3 (a_g)	1427	0
1292w	1048vw	−244	1294*s	1048w	−246	ν_5 (a_g)	1287	−257
1282w	1039vw	−243	1284*s					
1274m	1028vw	−246	1276*s	1027w	−249			
1259w	1015vw	−244	1261*s					
1184w			1185*m	837vw	−348	ν_{67} (b_{3u})	1152	−335
1174vw			1176*m					
	998w		1121w	999w	−122	ν_{47} (b_{2u})	1055	−74
			1113vw					
1014w	933w	−81	1005vw	934vw	−71	ν_6 (a_g)	979	−66
			976vw					
			918vw	901vw	−17	ν_{48} (b_{2u})	917	−15
			905vw	778vw	−127	ν_7 (a_g)	896	−108
888m	892m	+4	880s	887s	+7	ν_{49} (b_{2u})	898	−1
876w								
809vw			807w	744w	−63	ν_{50} (b_{2u})	876	−83
462m	461m	−1	456m	455m	−1	ν_9 (a_g)	508	0
442m	444m	+2	430m	433m	+3	ν_{10} (a_g)	438	−1
			308(RT)	303(RT)	−5	ν_{11} (a_g)	318	−2

[a] Reference 42.
[b] Reference 43.
[c] Reference 44.

four spectra (see Table I), since this is infrared-inactive in the isolated molecule. (Clearly, the CS vibration in the anion is not responsible for this large feature, since it occurs in other ET compounds. Furthermore, the anion CS vibration is usually weak.[44])

The third largest feature is the group near 450 cm^{-1}, which has been assigned by most authors to ν_9 (a_g) and/or ν_{10} (a_g). Certainly ν_9 (a_g) is calculated to have, along with ν_2 (a_g), the second-largest EMVC.[42]

Apart from the three strong features mentioned above, we observe many weaker features that seem to fit quite well into a pattern of other a_g and b_{2u} modes. The **E||c** features are more intense than the corresponding **E||b** features, because the mid-infrared electronic band is closer, and so we will refer mainly to Figs. 13 and 15. Starting from the highest wave number, the CH stretch doublet near 2900 cm^{-1} has been assigned to ν_1 (a_g), although ν_{44} (b_{2u}) and ν_{66} (b_{3u}), which are also CH stretches, are possible. Two sharp CN stretching lines are seen near 2100 cm^{-1} (see Figs. 7–11) due to the two distinct CN environments in the unit cell. Nakamoto[44] gives 2074 cm^{-1} for the CN stretch in a copper thiocyanato complex. Returning to Fig. 13, the pair of features near 1407 cm^{-1} has been assigned to ν_4 (a_g), assuming they shift to 1114 cm^{-1} in the d_8 spectrum. [Another candidate, ν_{45} (b_{2u}), has too large a calculated shift of 345 cm^{-1}.] The four strong lines, which are Fermi antiresonating with the broad ν_3 (a_g) in the protonated spectrum of Fig. 13, have been assigned with some confidence to ν_5 (a_g), which involves CH angle bends, on the basis of the observed isotope shift. The correlation and shift of the four lines is more convincing in the **E||b** spectra (see Fig. 14 and Table I). The reason for the quartet is simply because there are four molecules in the unit cell and there are four variations of the molecules vibrating in or out of phase together. Many of the modes appear as doublets, in which case they are either degenerate or unresolved. Modes appearing as singlets presumably are heavily damped so that their components form one broad feature [e.g., ν_3 (a_g)]. Two sharp features at 1185 and 1176 cm^{-1} have been assigned to ν_{67} (b_{3u}), since no other mode except the normally inactive ν_{14} (a_u) is calculated to appear in this region. They are Fermi-resonating with ν_3 (a_g) as evidenced by their comparative strength in Fig. 15 as the temperature changes. The assignment of the remaining features above 880 cm^{-1} in the lower curve of Fig. 13 is more speculative, but the continuation of the a_g modes (ν_6 and ν_7) and the b_{2u} modes (ν_{47} and ν_{48}) before ν_{49} at 880 cm^{-1} is fairly convincing (see Table I).

ACKNOWLEDGMENTS

The work at University of British Columbia (UBC) was supported by Grant No. 5-85653 from the Natural Sciences and Engineering Research Council (NSERC) of Canada. The work at Argonne National Laboratory was supported by the Office of Basic Energy Sciences, Division of Materials Sciences, of the U.S. Department of Energy, Contract No. W-31-109-Eng.-38.

[1]A. M. Kini, U. Geiser, H. H. Wang, K. D. Carlson, J. M. Williams, W. K. Kwok, K. G. Vandervoort, J. E. Thompson, D. L. Stupka, D. Jung, and M-H. Whangbo, Inorg. Chem. **29**, 2555 (1990).

[2]H. Urayama, H. Yamochi, G. Saito, K. Nozawa, T. Sugano, M. Kinoshita, S. Sato, K. Oshima, A. Kawamoto, and J. Tanaka, Chem. Lett. **1988**, 55 (1988).

[3]G. Saito, Mol. Cryst. Liq. Cryst. **181**, 65 (1990).

[4]K. Oshima, H. Urayama, H. Yamochi, and G. Saito, Physica C **153-155**, 1148 (1988).

[5]I. D. Parker, R. H. Friend, M. Kurmoo, P. Day, C. Lenoir, and P. Batail, J. Phys. Condens. Matter **1**, 4479 (1989).

[6]V. Z. Kresin and S. A. Wolf, Phys. Rev. B **41**, 4278 (1990).

[7]Y. J. Uemura, G. M. Luke, B. J. Sternlieb, J. H. Brewer, J. F. Carolan, W. N. Hardy, R. Kadono, J. R. Kempton, R. F. Kiefl, S. R. Kreitzman, P. Mulhern, T. M. Riseman, D. Ll. Williams, B. X. Yang, S. Uchida, H. Takagi, J. Gopalakrishnan, A. W. Sleight, M. A. Subramanian, C. L. Chien, M. Z. Cieplak, G. Xiao, V. Y. Lee, B. W. Statt, C. E. Stronach, W. J. Kossler, and X. H. Yu, Phys. Rev. Lett. **62**, 2317 (1989).

[8]K. E. Kornelsen, J. E. Eldridge, C. C. Homes, H. H. Wang, and J. M. Williams, Solid State Commun. **72**, 475 (1989).

[9]K. E. Kornelsen, J. E. Eldridge, H. H. Wang, and J. M. Williams, Solid State Commun. **74**, 501 (1990).

[10]K. E. Kornelsen, J. E. Eldridge, H. H. Wang, and J. M. Williams, Solid State Commun. **76**, 1009 (1990).

[11]R. E. Glover and M. Tinkham, Phys. Rev. **108**, 243 (1957).

[12]R. R. Joyce and P. L. Richards, Phys. Rev. Lett. **24**, 1007 (1970).

[13]G. Brändli and A. J. Sievers, Phys. Rev. B **5**, 3550 (1972).

[14]B. Farnworth and T. Timusk, Phys. Rev. B **10**, 2799 (1974).

[15]B. Andraka, J. S. Kim, G. R. Stewart, K. D. Carlson, H. H. Wang, and J. M. Williams, Phys. Rev. B **40**, 11 345 (1989).

[16]J. E. Graebner, R. C. Haddon, S. V. Chichester, and S. H. Glarum, Phys. Rev. B **41**, 4808 (1990).

[17]Y. Maruyama, T. Inabe, H. Urayama, Y. Yamochi, and G. Saito, Solid State Commun. **67**, 35 (1988).

[18]M. E. Hawley, K. E. Gray, B. D. Terris, H. H. Wang, K. D. Carlson, and J. M. Williams, Phys. Rev. Lett. **57**, 629 (1986).

[19]H. K. Ng, T. Timusk, D. Jerome, and K. Bechgaard, Phys. Rev. B **32**, 8041 (1985).

[20]K. E. Kornelsen, Ph.D. thesis, University of British Columbia, Vancouver, 1990.

[21]M. A. Biondi and M. P. Garfunkel, Phys. Rev. Lett. **2**, 143 (1959).

[22]K. Holczer, O. Klein, G. Grüner, H. Yamochi, and F. Wudl, in *Organic Superconductivity*, edited by V. Z. Kresia and W. A. Little (Plenum, London, 1990), p. 81. [Lower-Freqency data are found in Phys. Rev. Lett. **66**, 655 (1991).]

[23]K. Kamarás, S. L. Herr, C. D. Porter, N. Tache, D. B. Tanner, S. Etemad, T. Venkatesan, E. Chase, A. Inam, X. D. Wu, M. S. Hegde, and B. Dutta, Phys. Rev. Lett. **64**, 84 (1990).

[24]N. Toyota, T. Sasaki, K. Murata, Y. Honda, M. Tokumoto, H. Bando, N. Kinoshita, H. Inzai, T. Ishiguro, and Y. Muto, J. Phys. Soc. Jpn. **57**, 2616 (1988).

[25]G. Saito, Mol. Cryst. Liq. Cryst. **181**, 65 (1990).
[26]D. R. Harshman, R. N. Kleiman, R. C. Haddon, S. V. Chichester-Hicks, M. L. Kaplan, L. W. Rupp, T. Pfiz, D. Ll. Williams, and D. B. Mitzi, Phys. Rev. Lett. **64**, 1293 (1990).
[27]J. R. Ferraro, H. H. Wang, U. Geiser, A. M. Kini, M. A. Beno, J. M. Williams, S. Hill, M. H. Whangbo, and M. Evain, Solid State Commun. **68**, 917 (1988).
[28]M. G. Kaplunov, N. D. Kushch, and E. B. Yagubskii, Phys. Status Solidi A **110**, K111 (1988).
[29]K. Nishikida, H. Urayama, H. Yamochi, G. Saito, and M. Kinoshita, Phys. Rev. B **37**, 9100 (1988).
[30]T. Sugano, H. Hayashi, M. Kinoshita, and K. Nishikida, Phys. Rev. B **39**, 11 387 (1989).
[31]M. Tokumoto, H. Anzai, K. Takahashi, N. Kinoshita, K. Murata, T. Ishiguro, Y. Tanaka, Y. Hayakawa, H. Nagamori, and K. Nagasaka, Synth. Met. **27**, A171 (1988).
[32]A. Ugawa, G. Ojima, K. Yakushi, and H. Kuroda, Phys. Rev. B **38**, 5122 (1988).
[33]A. Ugawa, G. Ojima, K. Yakushi, and H. Kuroda, Synth. Met. **27**, A445 (1988).
[34]J. E. Eldridge and C. C. Homes, Infrared Phys. **29**, 143 (1989).
[35]D. Y. Smith, E. Shiles, and M. Inokuti, in *Handbook of Optical Constants of Solids,* edited by E. D. Palik (Academic, New York, 1985), p. 377.
[36]S. Gartner, E. Gogu, I. Heinen, H. J. Keller, T. Klutz, and D. Schweitzer, Solid State Commun. **65**, 1531 (1988).
[37]D. Jung, M. Evain, J. J. Novoa, M.-H. Whangbo, M. A. Beno, A. M. Kini, A. J. Schultz, J. M. Williams, and P. J. Nigrey, Inorg. Chem. **28**, 4516 (1989).
[38]K. Oshima, T. Mori, H. Inokuchi, H. Urayama, H. Yamochi, and G. Saito, Phys. Rev. B **38**, 938 (1988).
[39]K. Oshima, T. Mori, H. Inokuchi, H. Urayama, H. Yamochi, and G. Saito, Synth. Met. **27**, A413 (1988).
[40]H. Urayama, H. Yamochi, G. Saito, T. Sugano, M. Kinoshita, T. Inabe, T. Mori, Y. Maruyama, and H. Inokuchi, Chem. Lett. **1988**, 1057 (1988).
[41]J. E. Eldridge, J. Ren, and M.-H. Whangbo (unpublished).
[42]M. E. Kozlov, K. I. Pokhodnia, and A. A. Yurchenko, Spectrochim. Acta **45a**, 437 (1989).
[43]M. E. Kozlov, K. I. Pokhodnia, and A. A. Yurchenko, Spectrochim. Acta **43a**, 323 (1987).
[44]K. Nakamoto, *Infrared and Raman Spectra of Inorganic and Coordination Compounds* (Wiley, New York, 1986).
[45]J. E. Eldridge and Frances E. Bates, Phys. Rev. B **26**, 1590 (1982).
[46]C. C. Homes and J. E. Eldridge, Phys. Rev. B **40**, 6138 (1989).